

Enhanced EP halftones with hexagonal dot packing

*Tomasz J. Cholewo, Steve Weed, Brian Cooper and Michael Lhamon
Lexmark International, Inc.
Lexington, KY, USA*

Abstract

Hexagonal dot packing offers advantages for electrophotographic (EP) printing over conventional dot placement on a square grid. These advantages derive from a reduced neighborhood with which each dot interacts. Hexagonal dot packing has exhibited better grayscale performance with small clusters. Multiple dot centers in each tile allow obtaining more gray levels for a particular screen frequency. As a limiting case of multiple dot centers in a tile, stochastic screening on hexagonal and square grids is examined using a commercially available printing system. A novel method for comparing halftone spatial frequency components for all gray levels is demonstrated.

Keywords: hexagonal halftoning, spectrogram, stochastic screening

Introduction

A previous paper [1] reported that hexagonal dot packing could have some unique benefits for EP printing. These were thought to be largely a consequence of reduced dot size modulation from proximity of other dots, where each dot has eight other dots adjacent with square dot packing and only six with hexagonal.

Some questions unanswered in that investigation were:

- whether benefits were unique to a specific EP printer implementation;
- whether artifacts of the analysis methodology confounded the results;
- whether the benefits could be leveraged for halftones that reproduce grays with finer granularity.

For EP mechanisms with good spatial uniformity, some considerations for halftone design include:

- robustness of isolated dots and small clusters of dots for light tones;
- robustness of isolated voids and small void clusters for dark tones;
- monotonicity and even distribution of tone levels.

This last consideration can be somewhat discounted by increasing the halftone tile size.

Dot coverage and gray values

Paper commonly used for business EP printing typically has a CIE L^* measurement of around 93, which corresponds to about 83% of incident light being reflected. The first just-noticeably darker L^* value, 92, corresponds to about 80.7% reflection. If perfectly black dots were possible, then about 2.8% dot coverage would generate this just-noticeable difference. Real EP black prints measure about $L^* = 25$, which corresponds to about 4.42% reflection. About 2.9% dot coverage with this EP black would yield the same just noticeable difference.

At the other end of the scale, $L^* = 26$ corresponds to about 4.5% reflectance, which amounts to about 99.9% dot coverage with a 4.42% reflectance EP black. This suggests that, if isolated voids were comparable to isolated dots, halftone screens would need to be over 30×30 order to avoid contours in dark tones. This would result in lower than 40 line screens on a 1200 dpi printer, which would be unacceptably coarse. Consequently, it is beneficial for dot overlap to make isolated voids considerably smaller than isolated dots.

Disproportionate darkening is a concern in middle tones when the next dot to be printed connects previously isolated dots or clusters. One disadvantage of threshold array tiles that grow single dot clusters is that all clusters connect at the same time. Designing multi-cluster tiles for hexagonal dot packing should be somewhat simpler than for square dot packing, since one need only be concerned about connections with six adjacent dots instead of eight.

Spectrogram refinements

The spectrogram technique has been made more robust over the method used previously [1] for different image sizes, and FFT windows no longer overlap from one raster to the next. The results of multiple overlapping FFT windows applied to each image raster can optionally be combined, so that spectral data is more readily correlated to the original image. This optional reduction can be accomplished by averaging several FFTs or selecting the peak values for each component.

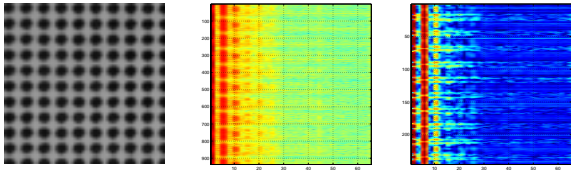


Figure 1: An example image and its old and improved spectrograms.

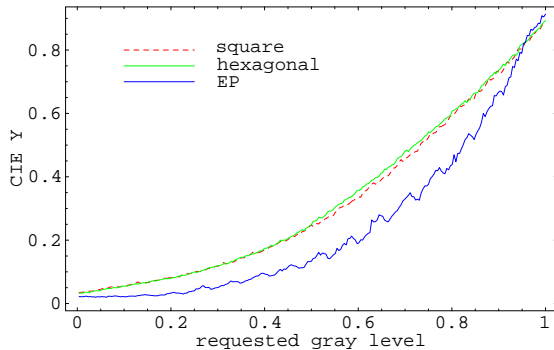


Figure 2: Comparison of reflectance in the function of gray level for square and hexagonal 1200 dpi halftones on PolaProof and on a desktop EP printer.

Peak values apply when one wants to retain the spectral sensitivity of a short FFT. This helps retain anomalies found in the spectral that would normally be washed out with a longer FFT window. However, averaging yields more stable and consistent spectra. Peaks appear if the anomaly is present throughout multiple windows. This is similar to a larger FFT window but it still more sensitive than a FFT of the entire raster line. We retain peak values for our analysis. A raw output is available but its output aspect ratio makes it difficult to print and read.

In addition to moving from a Matlab procedure to a standalone program accessible by more users, the algorithm refinements result in spectrograms of generally higher sensitivity with better locality. As an example, Figure 1 shows an image used previously and spectrograms of this image obtained using the old and new techniques, respectively. Spectrogram resolution was increased by collapsing all FFTs for an input scanline into a single spectrogram scanline, preserving peak values for each spectral component.

Stochastic halftone printing

Previously, spectrograms were generated from photomicrographic images of printed halftones using an NTSC video framegrabber. Hexagonal dot packing was implemented in a 600 dpi desktop EP printer. However encouraging those results may have been, their generality is certainly questionable. Hexagonal dots for this investigation are imple-

mented by printing bitmaps built from composite 1200 dpi dots on a 2400 dpi Polaroid PolaProof 1420 with square dot packing. A Nikon CoolPix 950 was used to capture 1200×1600 photomicrographs of these PolaProof prints. Because they are more perfectly square, the composite dots print with higher effective packing efficiency, and the PolaProof 1420 mechanism is inherently more robust against adjacent dot modulation than typical desktop EP printers. Consequently, the nature of this investigation is essentially a recomparison of hexagonal with square dot packing, having minimized all factors hypothesized to favor hexagonal. Figure 2 shows the measured CIE Y for all values of requested dot coverage. Printing with 100% dot packing efficiency and no dot gain mechanisms would result in a direct linear relationship between measured reflectance and requested dot coverage. The PolaProof square and hexagonal curves of Figure 2 are nearly linear for light and mid-tones, which would not be the case if dot sizes were being substantially modulated by adjacent dots. Reduced linearity for darker tones reflects that, after all, the real PolaProof dots are round and overlap substantially into adjacent voids.

Hexagonal printing was based on offset raster geometry shown in Figure 3a. The gradients evaluated for this poster were generated using a rotated hexagonal grid with offset columns, as depicted in Figure 4.

As an example of offset horizontal row dot packing implemented for a printer with square dot packing, consider Figure 3a, representing dots in a horizontal hexagonal grid. These can be realized on a square grid by increasing spacing horizontally and vertically as shown in Figure 3b. Figure 3c illustrates how each unique dot on the hexagonal grid is expanded into a 2×2 block on a square grid.

Just as in earlier work, the horizontal hexagonal grid is slightly asymmetric, with a value of $\alpha = 1$ for Ulichney's hexagonal packing aspect ratio. Grids of regular hexagons have grid aspect ratios of either $2/\sqrt{3}$ or $2\sqrt{3}$, which are optimal for round dots. Note that the grid aspect ratio is not the same as the aspect ratio between the longest and shortest diameters of the hexagon.

Offset sampled hexagons offer less covering efficiency for round dots than could be obtained with a grid of regular hexagons. Composite dots in this implementation are more nearly square than round, but the consequences of this sub-optimal implementation should be benign. On the other hand, minimizing dot size variability almost certainly limits the immediate practical applicability of these results for desktop business EP printers, but probably anticipates the results to be expected from inkjet printing, especially on coated substrates. Refining the bitmap scaling routine to better approximate typical printed dot behavior is a likely candidate for further research.

For some halftone techniques (e.g., error diffusion), the spatial frequency artifacts associated with particular con-

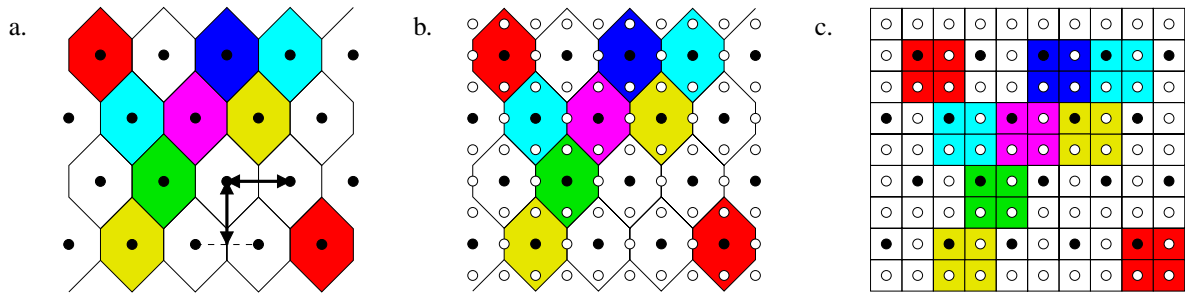


Figure 3: Emulation of horizontal hexagonal grid on a square grid device: a. hexagonal grid at 1200 dpi; b. square grid overlaid on hexagonal grid; c. 1200 dpi hexagonal dots on 2400 dpi square grid.

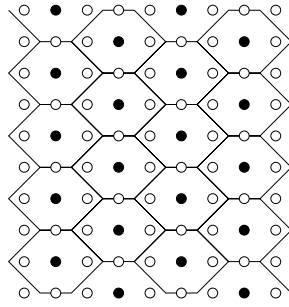


Figure 4: Hexagonal packing with vertical grid.

stant tone values cannot be extrapolated from a few samples. Therefore, we propose a strategy of performing vertical spectrograms on horizontal tone gradients and horizontal spectrograms on vertical tone gradients. These should provide more confidence in relative performance of different halftone and dot packing schemes from a comparatively small number of measurement samples. The random-appearing halftones used in these experiments are ordered (derived from a threshold array) with consistent and nearly isotropic spatial frequency attributes across the tonal range. Consequently, we ignore our own advice and provide only horizontal spectrograms for vertical tone gradients.

A Minimum Density Variance (MDV) algorithm [2] was used to generate a 128×128 hexagonal stochastic screen. Ulichney’s void-and-cluster algorithm [3] is based on a metric for isotropic spatial distances among dots in each dot profile, pruning the extreme instances by swapping dots from clusters into voids, while Minimum Density Variance applies a cost function to dot density variance in anisotropic regions (taking into account the anisotropic nature of human visual perception of structures) and locally permutes each region to minimize the cost of variance. For the examples in this poster, the threshold array for square dot packing was generated using void-and-cluster, while the hexagonal threshold array generated by Minimum Density Variance used circular regions and cost function to approximate the isotropic character of void-and-cluster.

MDV threshold values were calculated for the hexagonal dot centers on the square grid as in Figure 3b, comprising 25% of the locations within a 256×256 square array. Afterwards, each threshold value was expanded into a 2×2 block, as illustrated in Figure 3c.

An optimal Minimum Density Variance algorithm for square dot packing discriminates against vertical and horizontal dot structures, pushing problematic spatial frequency energy towards 45 and 135 degree diagonals. This improves image quality for halftones with square dot packing, but is suboptimal for offset sampled hexagonal dot packing, which has no fundamental vertical component, but does have diagonal structures that can be overly excited by anisotropic Minimum Density Variance algorithms.

The anisotropy of the MDV algorithm is controlled by the shape of the regions from which the cost of variance is accounted. Threshold arrays generated by anisotropic MDV have demonstrated an advantage over void-and-cluster arrays for square dot packing. This implies that a different region shape for hexagonal screens could minimize artifact structures associated with the angles among adjacent dot centers and exploit the inherent robustness of hexagonal dot packing against either vertical or horizontal artifact generation. Indeed, anisotropic optimization for MDV with hexagonal dot packing remains to be developed.

To render for a hexagonal screen, the input image needs also to be sampled onto a hexagonal grid. The square image at one resolution (e.g., 2400 dpi) was transformed into a hexagonal image at half the resolution (e.g., 1200 dpi) to accomplish this. For example, let Figure 3c represent a full resolution square image. Each pixel located at a black circle was expanded into a 2×2 block. For unbiased comparison, the square bitmap was similarly thresholded at half resolution. This technique is suitable for the gradients evaluated for this poster, but real images would be better served by, for example, cubic resampling of offset rows or columns.

Figure 5 shows the nominally square shape of PolaProof dots generated by bitmaps constrained to a 2×2 organization of the mechanism’s native round dots. Figure 5a

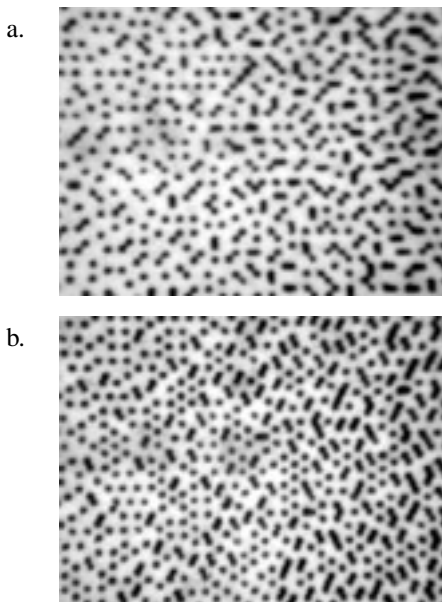


Figure 5: Nominally square dots at 1200 dpi formed by 2×2 clusters on PolaProof with a. square dot packing and b. hexagonal dot packing on a horizontal grid.

shows several instances of dot adjacency along diagonals with square dot packing, with composite square dots maintaining their shapes. Figure 5b shows bolder diagonal structures resulting from adjacent partially overlapped dots in a horizontal hexagonal grid. For many EP printers, the diagonal structures of Figure 5a would print on average nearly as boldly (but less consistently) as those in Figure 5b. The MDV algorithm used to generate the threshold array tile for Figure 5b was suboptimal in that it did not take into account the strength of diagonal structures as well as the weakness of visible structure for vertically adjacent dots in a horizontal hexagonal grid, relative to the square grid of Figure 5a.

Visual comparison of square and hexagonal screening

Natural images rendered with the hexagonal MDV screen were largely equivalent to the images rendered with the void-and-cluster square screen, except that the hexagonal screen tended to evidence filaments at the angles of the hexagonal grid. For the “horizontal” grid of Figure 3 the angles are $63 + 180k$ degrees and $27 + 90 + 180k$ degrees, for integers k . For the “vertical” grid of Figure 4 the angles are $27 + 180k$ and $63 + 90 + 180k$ degrees. (We assume that zero degrees direction points to the right, with positive angles in the counter-clockwise direction.) A comparison of bitmaps obtained by rendering an example image with a square and a hexagonal stochastic screens is shown in Figure 6.

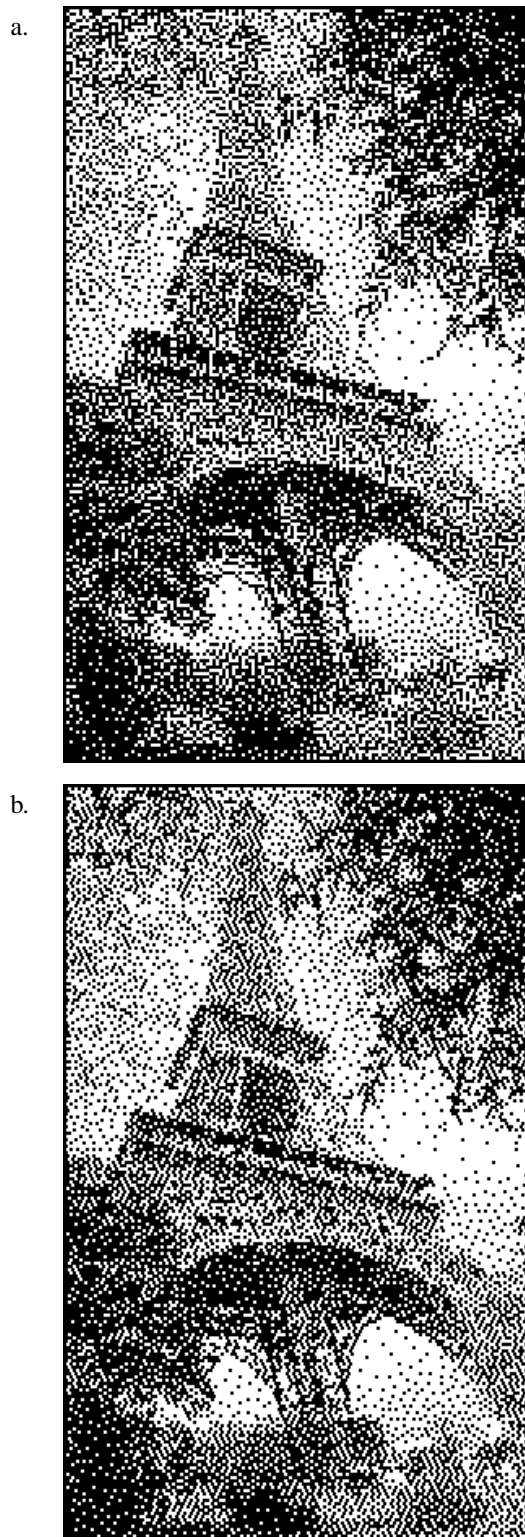


Figure 6: Image rendered with a. conventional (square) stochastic screen and b. hexagonal stochastic screen.

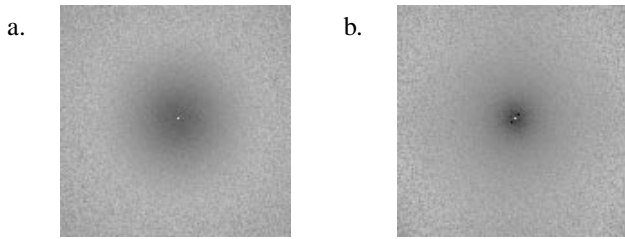


Figure 7: 2D FFTs of a. square and b. hexagonal threshold arrays.

Spectrogram and composite Fourier analysis

As explained above, 2×2 blocks of threshold values were created to implement the hexagonal grid. The square threshold array was also expanded by a factor of two, to minimize bias in comparison. In the frequency domain, the central half of the image closely matched the unscaled spatial image.

The composite Fourier transforms [4] for each stochastic screen were generated. In the frequency domain (Figure 7), the hexagonal screen has more low frequency energy than the square dot packing. This is consistent with our discussion of Figure 5.

Comparison of spectrograms from halftoned bitmaps with spectrograms from same-scale images captured from the printed bitmaps gives us a good indication of the validity of our procedures.

Both MDV and void-and-cluster halftones highlight a limitation of spectrogram halftone analysis, in that spectrograms show relatively constant spectral energy, while 2D FFTs show reduced energy at lower frequencies. These halftone algorithms take into account that human perception of visual structures is two dimensional and that lower frequency structures are more visible. Even if not obviously periodic, appreciable low frequency artifacts can be considered objectionably grainy. Consequently, halftones whose spectrograms contain low frequencies may or may not be problematic, since correlation of dots in the orthogonal direction is not addressed.

The proofer prints 2400 dpi bitmaps, and digitally enlarging bitmaps two times results in a 1200 dpi prints with square dots having relatively little dot gain. Photomicrographic images of these proofs can be compared to their digital bitmaps. There are high frequency components in the bitmaps corresponding to the ideal binary dot response which are not present in the optical capture of the printed proofs, but these are fairly easy to identify in the spectrograms and discount.

The lack of apparent periodic structure in the halftoned bitmaps is reflected in the broader spatial energy distribution in the spectrograms of Figures 8 and 9, compared to spectral bands for clustered dot halftone screens. The bitmap spectrograms show evenly distributed spatial fre-

quency energy up to nearly the dot width. The comparable photomicrographs of Figures 10 and 11 show significant loss of higher frequencies. Both printing and image capture contribute to this attenuation of energy at higher frequencies.

These images are vertical gradients from black at the bottom to white at the top. The spectrogram program calculates 1D FFTs along image raster lines, so each spectrogram scanline is generated for a constant dot coverage value. As might be expected, the spectrograms show more broadband spectral energy for middle tones than near solid white or black.

The photomicrographs were captured with 1600 raster lines, while the bitmaps contain 1024 raster lines, with each print dot generated by a 2×2 square of pixels. For easier comparison, the photomicrographs were rescaled to 1024 raster lines using Photoshop's bicubic resampling, which is known to add moderate sharpening. A good deal of the high frequency spatial energy is lost in the processes of printing the bitmaps and capturing images of those prints. For example, the spectrograms in Figures 8 and 9 show significant energy for frequencies corresponding to $k > 250$. The spectrograms use FFT and Hanning Window lengths of 512, so maximum $k = 256$ corresponds to two pixels, which is the width of a composite 1200 dot. The spectrograms of Figures 10 and 11, derived from image capture of prints of these bitmaps, show spatial frequency energy dropping above $k = 128$. This is consistent with replacing perfect binary dot density transitions with Gaussian spreading. Since the unaided human eye cannot distinguish whether a 1/1200 inch dot has binary or Gaussian density, spatial energy above the dot frequency ($k \approx 128$) is of little interest, except in cases where it may be aliased with image information.

The spectrograms of Figures 10 and 11 also show faint, nearly vertical lines corresponding to a spectral component around $k = 213$. We calculated that this $k = 213$ artifact results from aliasing between the printed halftone and the digital camera sensor array.

Conclusions

The good news is that hexagonal dot packing appears to have no appreciable print quality disadvantages in comparison to square dot packing, even when the dot formation mechanisms that would favor hexagonal dot packing are minimized. Inverting this logic supports our hypothesis that hexagonal dot packing can be beneficial when dot size is modulated by the proximity of other dots. Since this effect is orthogonal to its more commonly cited theoretical advantages, such as improved pixel packing efficiency and higher apparent resolution for a given pixel density, the case for hexagonal dot packing becomes more persuasive with decreasing cost of halftoning images with square

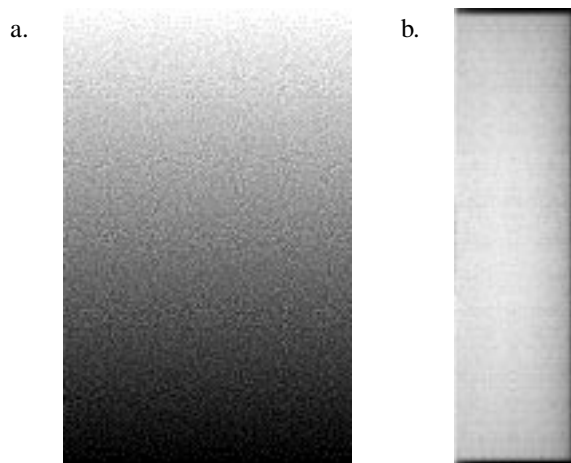


Figure 8: Bitmap and spectrogram for square dot packing for 1200 dpi printing on a 2400 dpi PolaProof.

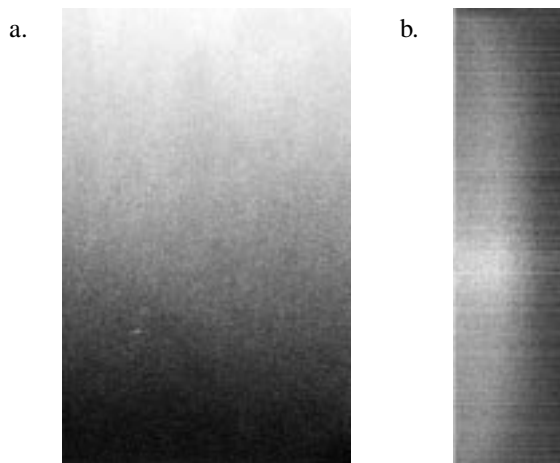


Figure 10: Photomicrograph and spectrogram of PolaProof gradient using 1200 dpi square dot packing.

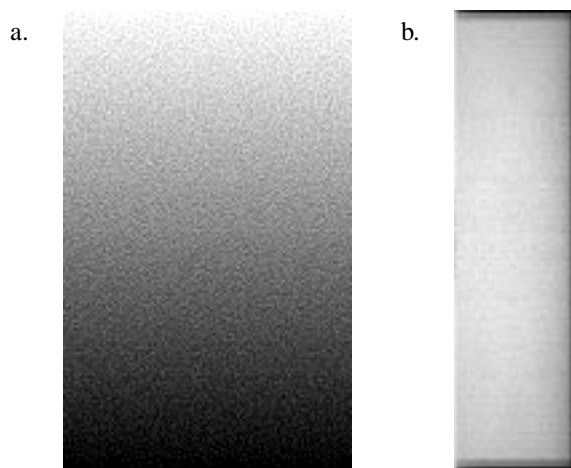


Figure 9: Bitmap and spectrogram for hexagonal dot packing on a vertical grid.

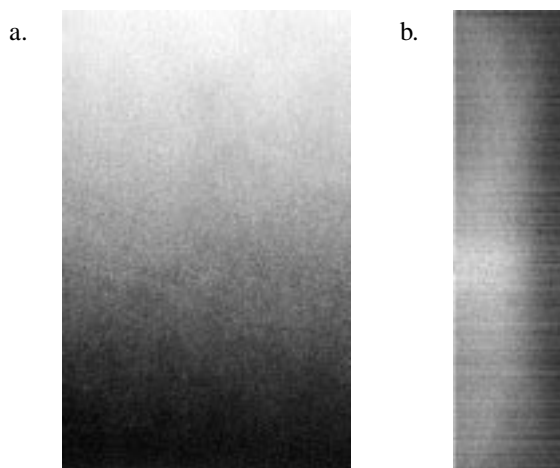


Figure 11: Photomicrograph and spectrogram of PolaProof gradient using 1200 dpi hexagonal dot packing on a vertical grid.

pixel packing to dots with hexagonal pixel packing.

Future investigations could include:

- better accounting for artifacts of printed image capture.
- preprocessing bitmaps so that 2400 dpi proofer prints simulate those from lower resolution printers;
- optimizing the MDV cost function for hexagonal dot packing;
- cubic resampling for images halftoned with hexagonal dot packing.

References

[1] M. Turbek, S. Weed, T. J. Cholewo, B. Damon, and M. Lhamon. Comparison of hexagonal and square dot centers for

EP halftones. In *IS&T PICS: Image Processing, Image Quality, Image Capture Systems Conference*, pages 321–325, Portland, Ore., March 2000.

[2] B. E. Cooper, T. A. Knight, and S. T. Love. Method for halftoning using stochastic dithering with minimum density variance. U.S. Patent No. 5,696,602, 1997.

[3] R. A. Ulichney. The void-and-cluster method for dither array generation. In B. E. Rogowitz and J. P. Allebach, editors, *Proceedings SPIE, Human Vision, Visual Processing, Digital Displays IV*, volume 1913, pages 332–343, February 1993.

[4] R. Ulichney. *Digital halftoning*. MIT Press, Cambridge, Mass., 1987.